CHEMISTRY OF MATERIALS

pubs.acs.org/cm

Article

Unraveling Molecular Design Principle of Ferroelasticity in Organic Semiconductor Crystals with Two-Dimensional Brickwork Packing

Sang Kyu Park,*,# Hong Sun,# Michael Bernhardt, Kyoungtae Hwang, John E. Anthony, Kejie Zhao,* and Ying Diao*

Cite This: *Chem. Mater.* 2023, 35, 81−93

Read Online

ACCESS | Metrics & More | Article Recommendations | Supporting Information

ABSTRACT: Ferroelasticity of organic single crystals has recently attracted great research interest. It is a reversible twinning transition in response to mechanical stress that imparts remarkable deformability to crystalline materials while allowing materials to retain their inherent functional properties. These appealing attributes of ferroelasticity promise high-performance ultraflexible, stretchable single-crystalline (opto-) electronics. In this work, we unravel structural criteria for ferroelastic transition of trialkylsilyl-acene (TAS-acene) crystals, which are known as high-performance organic semiconductor materials owing to two-dimensional electronic coupling. This study unveils that ferroelastic transitions are achievable only if two-dimensional brickwork packing is absent from both neighboring aromatic core and TAS side-chain interlocking. This is because aromatic core interlocking prevents cooperative molecular gliding and rotation during structural transition, while side-chain interlocking prevents TAS side-chain reconfiguration necessary for relieving steric strain occurring upon the cooperative molecular motions. The correlation of molecular arrangement and ferroelastic transition capability revealed herein will provide insight into the material design principle of inherently flexible organic semiconductor crystals.

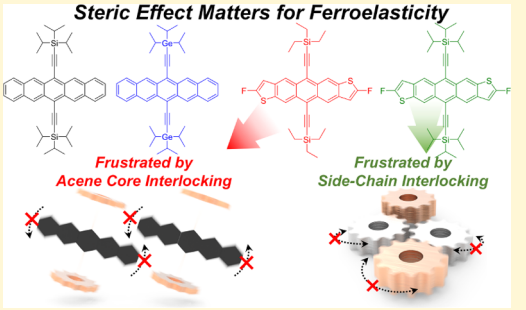

INTRODUCTION

Martensitic transition, formerly proprietary to metals, alloys, and ceramics,[1−5] has recently been expanded to the realm of molecular crystalline materials.[6−42] Martensitic transition is generally a displacive and highly reversible polymorphic or twinning transition achieved by cooperative molecular motions.[43] Such a martensitic/cooperative transition is a prominent underlying principle for fascinating dynamic responses of materials to thermo-mechanical stimuli (i.e., crystal adaptronics),[44] such as thermosalient effects and super- and ferroelasticity.[45,46] By thermosalient effects, molecular crystals represent remarkable actuation behaviors—for example, jumping, bending, or twisting motions, enabled by the sudden release of the elastic strain energy accumulated during the martensitic transition.[6−15] By super- and ferroelasticity, molecular crystals become reversibly deformable beyond the elastic limit upon mechanical loading, where the superelastic crystals recover shape through spontaneous reverse transition upon unloading while ferroelastic crystals do so by applying opposite shear stress. Such intriguing attributes of martensitic molecular crystals engender excellent application potential toward smart sensors,[21] actuators,[15,16] lifts,[19] and high-performance ultraflexible[33] and shape memory optoelectronic devices.[29]

To date, only a handful of molecular crystals are revealed to show martensitic transitions.[46] The discoveries have been mostly serendipitous. In the studies carried out so far, molecular level understandings of how the cooperative transitions occur have been provided; the most probable molecular motions that underline the martensitic transitions have been suggested by resolving crystal structures before/after transitions. However, the reverse design question is left unanswered: what is the molecular/crystal engineering principles for devising martensitic molecular crystals? Addressing this question requires systematic variation of molecular structures and such studies remain rare. However, there are a few notable examples. For instance, Takamizawa and co-workers elucidated odd−even carbon number dependence of superelasticity in fatty acid crystals; superelasticity is observed only in odd-numbered fatty acids but not in even-numbered cases, where the latter requires excessive molecular conformation change that prevents superelastic transitions.[20] Moreover, we have recently revealed that single atomic substitution in the rotator side chains of benzothieno[3,2-*b*]benzothiophene derivatives from $-C(CH_3)_3$ to $-Si(CH_3)_3$

Received: August 17, 2022
Revised: December 13, 2022
Published: December 21, 2022

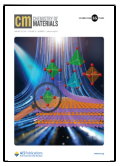

led to stronger side-chain-to-side-chain and side-chain-to-core interactions and thus prevented dynamic side-chain rotation and inhibited martensitic transition.[30,32] Furthermore, Ito and co-workers not only demonstrated ferroelastic luminescent crystals but also revealed structural factors (i.e., steric repulsion of bulky unit and molecular alignment in the packing structure) that determine twinnability in a series of structurally similar N-heterocyclic gold complexes.[47] These examples illustrate that even the slightest change in the molecular structure can completely modify transition characteristics by altering molecular packing and strength of intermolecular interactions.[20,30,32,47]

In this report, we unravel important structural criteria that facilitate/prevent ferroelastic transitions of trialkylsilylethynyl (TAS)-functionalized (hetero-)acenes featuring two-dimensional (2D) brickwork packing.[48−50] This class of molecules, which Anthony and colleagues originally designed, can foster brickwork packing with 2D electronic coupling that allows efficient charge carrier transport. Moreover, we recently found for the first time that 6,13-bis(triisopropylsilylethynyl)-pentacene (TIPS-P) exhibits ferroelasticity which enabled ultraflexible single-crystal electronics application.[33,34] However, in our previous work, the key question of molecular/structural origin underpinning ferroelastic transitions of TIPS-P remains unanswered. In this work, we address this question by investigating the capability of ferroelastic transitions in 2D brickwork packing TAS acenes, a series of TIPS-P analogues with systematically varied side chains and acene cores.[51,52] We find that cooperative molecular displacement/rotation and reconfiguration of side chains that are responsible for ferroelastic transition can be promoted when interlocking of the aromatic core and rotator side chain is alleviated.

MATERIALS AND METHODS

Materials. TIPS-P, 2,8-difluoro-5,11-bis(triethylsilylethynyl)-anthradithiophene (diF-TES-ADT), toluene, methanol, ethanol, butyl acetate, heptane, and octadecyltrichlorosilane are purchased from Sigma-Aldrich and used as received. 6,13-Bis(triisopropylgermanylethynyl)pentacene (TIPGe-P) and 2,8-difluoro-5,11-bis(triisopropylsilylethynyl)anthradithiophene (diF-TIPS-ADT) are synthesized according to the methods reported previously.[51,52] The chemical structures of products are confirmed by ^{1}H NMR and matrix-assisted laser desorption ionization time-of-flight (MALDI-TOF) (Figures S1 and S2).

Instruments. ^{1}H NMR spectra are obtained using an Agilent solution state NMR 600 MHz spectrometer. MALDI-TOF spectra are obtained using a Bruker Microflex instrument. Cross-polarized microscopy (CPOM) images are taken using a Nikon Eclipse Ci-POL optical microscope equipped with a high-speed camera (Infinity 1, Lumenera Corp.). For variable temperature in situ CPOM study, a Linkam LTS420 stage is employed. (Polarized) Raman spectra are obtained using a Horiba Raman confocal imaging microscope (LabRAM HR 3D) with 785 nm (diF-TES-ADT) and 832 nm laser (TIPS-P, TIPGe-P) excitation sources (50× long working distance objective lens). Diffraction data of TIPGe-P twinned crystals are collected using a Bruker D8 Venture equipped with four-circle kappa diffractometer and Photon 2 detector.

Crystal Growth. TIPS-P and diF-TIPS-ADT crystals are grown based on vapor diffusion method. The vials containing TIPS-P and diF-TIPS-ADT toluene solution (8 mg mL^{-1}) are placed in the methanol baths. The baths are placed at ambient temperature, in a dark state, until the crystals grow to a sufficient size. The crystals are filtered and collected after the growth process. 2D brickwork packing TIPGe-P crystals are grown based on drop-casting, following the method reported by Sorli et al.[51] TIPGe-P solution (12 mg mL^{-1}) based on 1:1:1 butyl acetate/toluene/heptane mixture solvent is drop-cast onto an octadecyltrichlorosilane-treated indented plate. After the solution is completely dried, the crystals are separated from the plate by dispensing ethanol over it. The crystals are filtered and dried before use. To isolate the 2D brickwork packing TIPGe-P crystals, however, it requires special attention. The previous report has shown that TIPGe-P produces multiple polymorphs, that is, herringbone, 2D brickwork, and slipped stack polymorphs, the first two of which are the major products in this procedure.[51] However, it is found through CPOM, powder X-ray diffraction, and single-crystal X-ray diffraction (SC-XRD) studies that they have distinct morphologies. Specifically, herringbone crystals have a bulky rectangular shape, while 2D brickwork crystals have a ribbon shape (Figure S3a,b). For 2D brickwork case, it is discovered that these crystals exhibit a particular angle of about 50° at the ribbon tip (Figure S3a) due to the manifestation of the (100) and (110) planes indexed by SC-XRD (Figure S4). Based on this observation, we separate the crystals by their morphologies, confirm phase purity by powder X-ray diffraction patterns (Figure S3c), and utilize ribbon-shaped 2D brickwork crystals in this study. diF-TES-ADT crystals are grown by sublimation method. The dish containing diF-TES-ADT powder is covered with the target substrate (Si/SiO_2 or glass) and heated at 180 °C until the powder is completely sublimed. The target substrate with diF-TES-ADT crystals is cooled slowly before use. The sublimation growth procedures are carried out in an N_2-filled glovebox.

Investigation of Ferroelastic Transition Capability of TAS-Acene Crystals Based on Mechanical Loading. For TIPS-P, TIPGe-P, and diF-TIPS-ADT crystals with sufficient thicknesses ($t \geq 3$ μm), direct mechanical shearing tests are performed. As previously reported, we build freestanding jumping board configuration using these crystals.[33] A piece of microscope cover glass is attached to the SiO_2/Si substrate; then about half of the crystals are placed on the cover glass. The crystal is then fixed with a small amount of epoxy glue to allow another half of the crystal to be floated. After the completion of curing (ca. 8 h, RT), the crystal is mechanically sheared using a micromanipulator probe. To note, it is difficult to exert direct shear to flexible thin crystals ($t \leq 3$ μm) because they are easily bent or twisted when in contact with the micromanipulator probe. Therefore, thicker crystals ($t \geq 3$ μm) that are devoid of unwanted deformations are employed in this experiment.

In addition to the direct shearing, direct mechanical tension tests of these crystals are performed by bending.[33] For this, the crystals are placed on polyethylene terephthalate (PET, 330 μm in thickness) substrates, and both ends of the crystals are fixed with epoxy glue. After the completion of curing, the substrates with crystals are bent convexly, resulting in tension along the long axis of crystals.

Investigation of Ferroelastic Transition Capability of TAS-Acene Crystals Based on Thermal Annealing. In this experiment, we place thin TAS-acene crystals with a clean surface onto SiO_2/Si substrates because good adhesion between crystals and substrates is a prerequisite to induce ferroelasticity by the method. Taking TIPS-P as a representative example, crystals with a thickness less than 10 μm show good adhesion to the substrates at room and/or high temperature, tested by pushing the crystals by using a Nylon wire. In the next step, the samples are heated up to target temperature, followed by subsequent cooling. The heating and cooling rates are set to 10 or 20 °C/min, respectively, and there seems to be no particular difference in the results. In the case of TIPS-P and TIPGe-P, the crystals are heated up to slightly above low-temperature (LT) to high-temperature (HT) phase transition temperature, that is, 200−220 °C (TIPS-P) and 140−150 °C (TIPGe-P), considering that the transition temperatures observed by differential scanning calorimetry (DSC) studies are reported as 180−200 °C (TIPGe-P) and 125−145 °C (TIPGe-P).[33,51] Meanwhile, the transition temperature difference (DSC vs variable temperature microscopy) may come from the hot stage configuration; the slide glass capable of micromanipulation is placed on the heating element in the Linkam LTS420 stage that we employed; thus, there may be imperfect contact between these elements. By LT-to-HT phase transition, the crystals are elongated up to about 16 and 13%. Upon consecutive cooling process, elongated HT crystals maintain shape/strain by deformation twinning because

https://doi.org/10.1021/acs.chemmater.2c02534
Chem. Mater. 2023, 35, 81−93

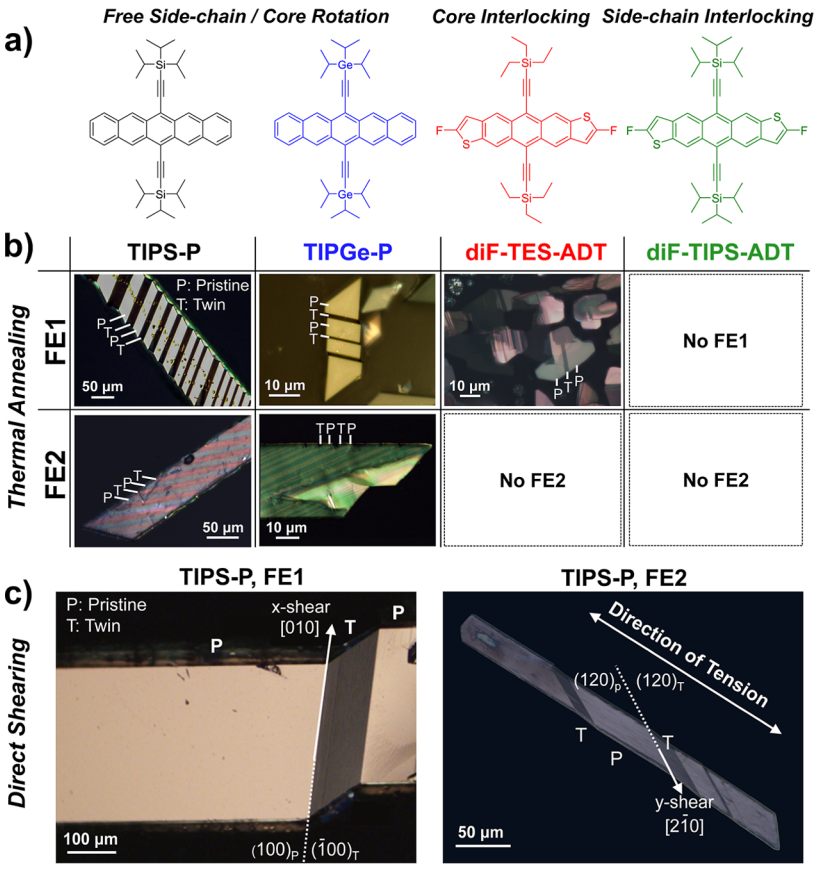

Figure 1. (a) Molecular structures of TIPS-P, TIPGe-P, diF-TES-ADT, and diF-TIPS-ADT. (b) Observed ferroelastic transitions (FE1 and FE2) by thermal annealing in the molecular crystals of TIPS-P, TIPGe-P, diF-TES-ADT, and diF-TIPS-ADT and their cross-polarized micrographs. (c) Cross-polarized optical micrographic images of twinned TIPS-P under *x*-shear (left) and *y*-shear (right). The *y*-shear in (c) is accomplished by applying tension along the long axis of the crystals.

strong adhesion between crystals and the substrate restricts shape restoration (i.e., strain accommodation). Shape preservation upon HT-to-LT phase transition is one of the unique features of shape memory alloys, which is also known as strain accommodation behavior. In the case of diF-TES-ADT and diF-TIPS-ADT crystals that do not undergo martensitic transition between ambient temperature and melting temperature, the crystals are heated up to about 10−20 °C below the melting temperature, ca. 200 °C (diF-TES-ADT) and 175 °C (diF-TIPS-ADT), respectively. Despite the absence of polymorphic transition accompanying staggering crystal elongation, these crystals are expanded enough (2−4%, measured by optical microscopy) under the high-temperature conditions and therefore mechanically strained beyond the elastic limit upon cooling process.

Single Crystal X-ray Diffraction. Diffraction data of a twinned crystal of TIPGe-P were collected on a Bruker D8 Venture equipped with a four-circle kappa diffractometer and Photon 2 detector. The Iμs microfocus Mo (λ = 0.71073 Å) source supplied the multi-mirror mono-chromated incident beam. Data were collected as a series of φ scans at 300 K. Based on the collected data, the facets of pristine and twinned domains were indexed using APEX3, Bruker (2018). Employing Cell Now (Sheldrick, 2008), the orientational relationship between the pristine and twinned domains was analyzed.

Raman Spectra Calculation. Geometry optimizations and Raman spectra thereof are calculated using Gaussian 09 software package. We employ B3LYP functional and 6-311g(d) basis set, which are implemented in Gaussian 09. A scaling factor of 0.966 is applied to calculated vibrational frequencies, alloying them better match the experimental spectra.

Atomistic Simulation. The simulation details for large-scale molecular dynamics (MD) on the FE1 and FE2 of TIPS-P are available in our recent paper.[33]

The ferroelastic transitions of diF-TES-ADT and diF-TIPS-ADT are investigated by applying the DFT simulation onto the 2 × 2 × 1 supercell. The supercell model, containing 304 and 376 atoms, respectively (four molecules), is built by expanding the optimized unit cell obtained from the XRD experiment. The calculations are carried out based on the hybrid Gaussian and plane waves scheme implemented in the CP2K package.[53] The DZVP molecularly optimized basis sets[54] and a 400 Ry cutoff auxiliary plane-wave basis set[55] are employed, with accompanying Goedecker−Teter−Hutter pseudopotentials.[56] The exchange and correlation term is treated by the PBE functional with the DFT-D3 correction.[57,58] At 27 °C, the shear-induced FE1 and the tensile-induced FE2 are accomplished by the ab initio MD (AIMD) simulation with the aid of the quasi-static loading algorithm. Basically, we apply the incremental 1% shear strain ε_{xy} or tensile strain ε_{yy} onto the supercell model at each step, and afterward, the model undergoes the ab initio MD in the canonical ensemble *NVT* for 1 ps at each strained state. After that, the lattice structures obtained from the dynamic transition will be fully relaxed and optimized until the atomic displacements are lower than 1.6 × 10^{-4} nm and forces on the atoms are smaller than 0.23 eV/nm. The temperature is controlled using the generalized Langevin thermostat with the time step of 0.5 fs, and all periodic boundary conditions are adopted in the DFT simulation.

RESULTS AND DISCUSSION

Ferroelastic Transitions in TAS-Acene Analogues. Figure 1a presents molecular structures of TIPS-P and its analogues—TIPGe-P, diF-TES-ADT, and diF-TIPS-ADT,

https://doi.org/10.1021/acs.chemmater.2c02534
Chem. Mater. 2023, 35, 81−93

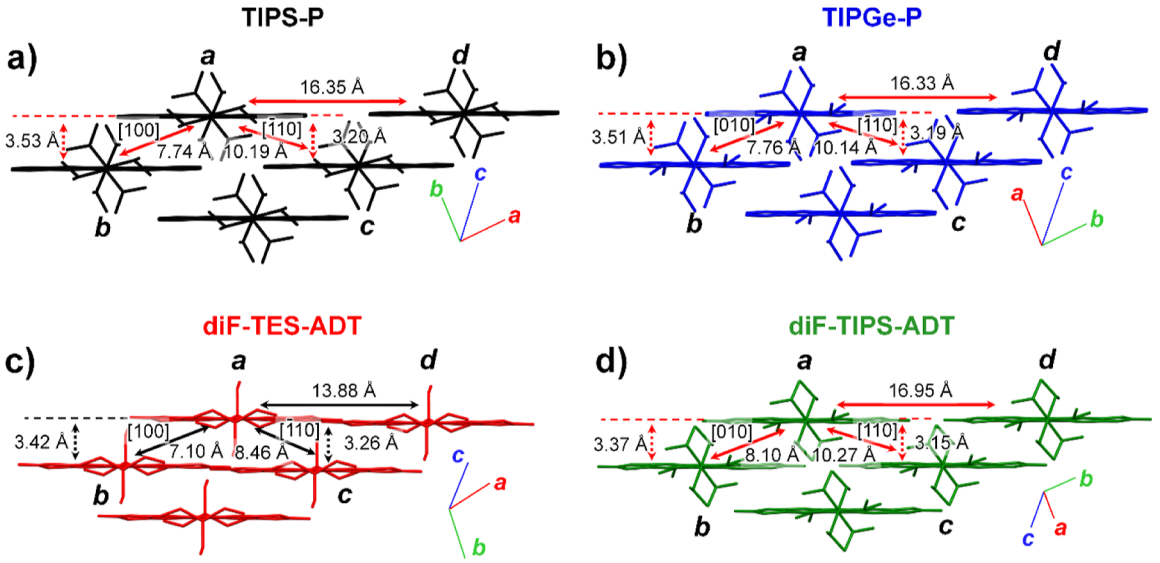

Figure 2. Comparison of molecule packing of (a) TIPS-P, (b) TIPGe-P, (c) diF-TES-ADT, and (d) diF-TIPS-ADT. Inter π-plane distances and centroid-to-centroid distances are indicated with dotted and solid arrows, respectively.

which are of interest in this work. In order to scrutinize their ferroelastic transition capabilities, we exert stress on crystals in two different ways: direct mechanical shearing and thermal annealing (Figure 1b,c). In both cases, all the analogues are strained above the elastic limit (strain < 2%), which is approximated by the direct tensioning case of TIPS-P crystals (Figure S5). Based on the shearing direction, the crystals can undergo two different types of twinning modes—that is, ferroelasticity 1 (FE1) and ferroelasticity 2 (FE2). Exerting x-shear onto the crystal creates a twinned domain by FE1, while exerting y-shear accomplished by tensioning along the long axis of the crystal creates a twinned domain by FE2 (see Figure 1c for TIPS-P cases). As previously reported, TIPS-P crystals undergo both FE1 and FE2 transitions with recoverable shear strain of 59.9%, enabling ultraflexible single-crystalline electronic device applications.[33,34] Applying an x-shear causes FE1 transition, which is accomplished by 180° rotation of the lattice against (100) twin plane normal (Figure 1c, left). Meanwhile, applying an y-shear causes FE2 transition, which is accomplished by a 180° rotation of the lattice against $[2\bar{1}0]$ vector (Figure 1c, right).

Interestingly, due to strain self-accommodation behavior, the same twinning phenomena (FE1 and FE2) can be attained after thermal annealing (Figure 1b). Here, the strain self-accommodation, which has been a unique feature of shape memory alloys, refers to the preservation of the elongated shape of the high-temperature phase by twinning transition that occurs during cooling process. To facilitate such behavior, we place thin crystals with the clean surface (thickness, $t \leq 10$ μm) onto SiO_2/Si substrates. As presented in Movie S1 and S2, these crystals show good adhesion to the substrates at room and/or high temperature because the flexibility of thinner crystals enables conformal contact with the clean substrates.[59−61] Specifically, a thin crystal ($t \leq 3$ μm) readily adheres to the substrate at room temperature and does not move at all when pushed using a Nylon wire, while a crystal of moderate thickness ($6.8 \leq t \leq 10$ μm) exhibits good adhesion only at a high temperature, at which the crystal becomes more malleable due to HT phase formation. However, a thick crystal ($t \sim 20$ μm) does not exhibit strong adhesion even at high temperature. The formation of adhesion is strongly correlated with the ferroelastic transition capability during the cooling step. As shown in Movie S3, only the crystals with strong adhesion develop twin domains upon cooling. Therefore, it should be emphasized that the method is particularly useful when examining the twinning capability of thin crystals to which direct shear is difficult to apply. However, it should also be noted that both FE1 and FE2 transitions can be induced by the method, although their incidence is found to be stochastic. We believe that the direction of local shear plays a pivotal role in determining whether FE1 or FE2 will occur, which is likely to be affected by how a crystal is attached to a substrate.

By the same methods, we test ferroelastic transition capabilities of the analogue crystals. Like TIPS-P crystals, TIPGe-P crystals undergo FE1 (FE2) transition when subjected to x-shear (y-shear), as shown in Figure S6. Moreover, thermal annealing and subsequent cooling of TIPGe-P induce both FE1 and FE2 transitions (Figure 1b). As shown in Movie S4 and Figure S7a,b, TIPGe-P crystals show phase transition in the temperature range of 125−140 °C upon heating, where phase boundary sweeping behavior is clearly manifested. Moreover, the structural integrity of the crystals is well preserved during the transition, despite the fact that the crystals are elongated by 12.9%. Based on the observations, we conclude that TIPGe-P is capable of thermoelastic transition. Interestingly, we observe that the elongated shape is maintained upon subsequent cooling, attributed to the ferroelastic transition occurring in this process (Movie S4).

However, because the crystals are too thin to be sheared directly, twinning capabilities of diF-TES-ADT crystals are only examined by thermal annealing. As presented in Figure 1b, after thermal annealing of diF-TES-ADT crystals, only FE1 type twins are observed. On the contrary, single crystals of diF-TIPS-ADT exhibit brittle fracture upon application of direct shear or after thermal annealing (Figure S8). It should be herein noted that diF-TES-ADT and diF-TIPS-ADT crystals do not exhibit thermoelasticity before melting. Instead, they show changes in length by thermal expansion (Figure S7c−f, diF-TES-ADT: 2.4% at 220 °C; diF-TIPS-ADT: 4.5% at 200

https://doi.org/10.1021/acs.chemmater.2c02534
Chem. Mater. 2023, 35, 81−93

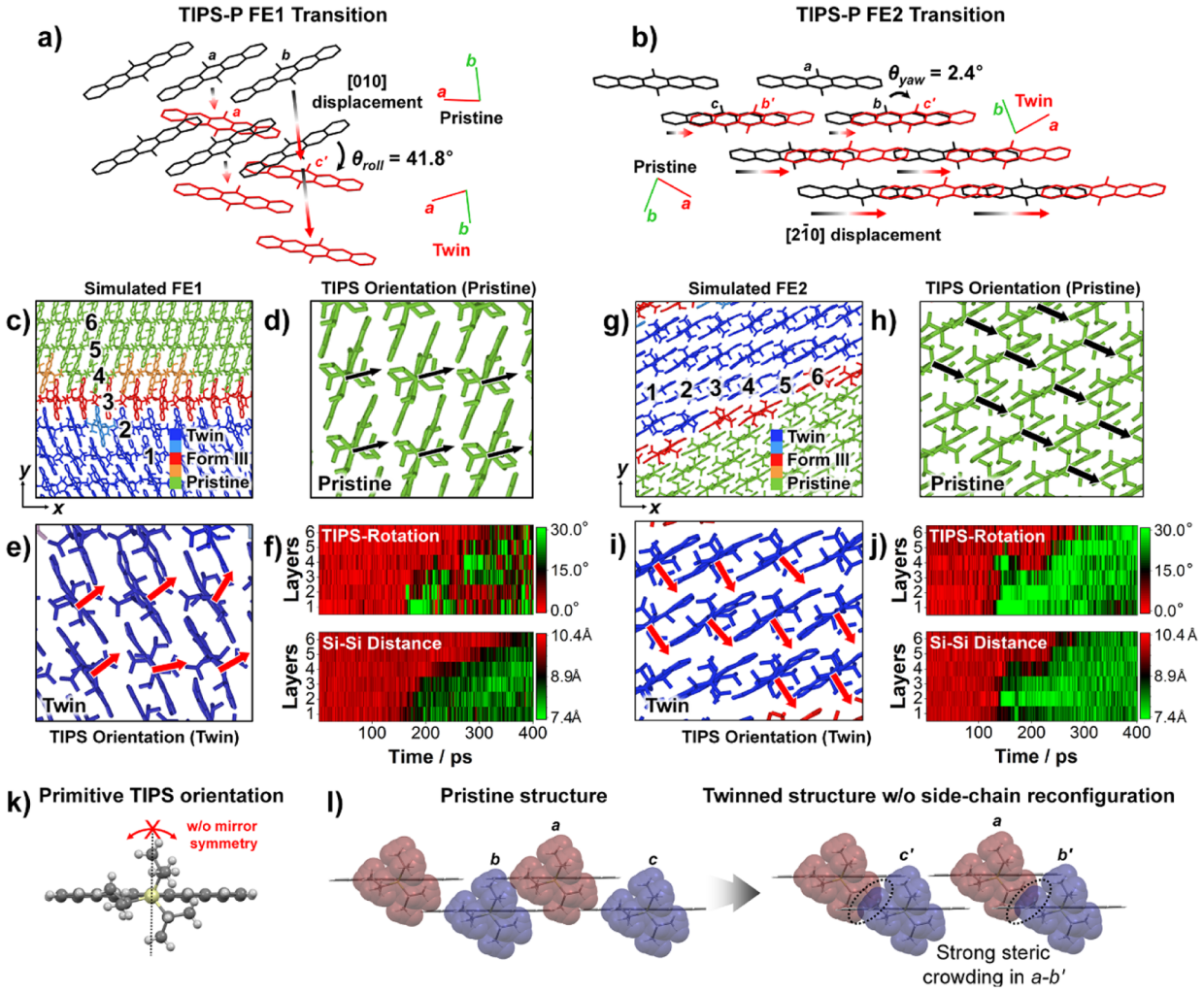

Figure 3. Ferroelastically transformed structure of TIPS-P by (a) FE1 and (b) FE2 process (black: pristine structure; red: twinned structure). Due to the π-stacking axes switching mechanism, $a-b$ pair becomes $a-c'$ pair and vice versa by ferroelastic transition. (c) MD simulated FE1 structure by x-shearing showing pristine (green), Form III interface (red), and twinned domain (blue). TIPS orientation in the (d) pristine and (e) twinned domain, indicated with black and red arrows, respectively. (f) TIPS rotation angle vs time contour plot (top) and Si−Si distance vs time contour plot (bottom) of six different molecules in adjacent layers [1−6 of (c)]. (g) MD simulated FE2 structure by tensile loading (y-shear) showing pristine (green), Form III interface (red), and twinned domain (blue). TIPS orientation in the (h) pristine and (i) twinned domain, indicated with black and red arrows, respectively. (j) TIPS rotation angle vs time contour plot (top) and Si−Si distance vs time contour plot (bottom) of six different molecules in adjacent layers [1−6 of (g)]. Upon structural transformation in (f,j) (validated from distance change between neighboring TIPS-units, $a-c$ pair), substantial rotations in the side chains are shown by color evolution from red to green. (k) Molecular structure found in the crystal structure of TIPS-P, which exhibits specific orientation of TIPS unit without mirror symmetry with respect to the plane perpendicular to backbone (black dotted line). (l) Attributed to the primitive side-chain orientation, steric hindrance in a-b′ increases at the transformation boundary.

°C). Given that diF-TES-ADT and diF-TIPS-ADT crystals undergo FE1 and fracture, respectively, such elongations are sufficient to apply strain beyond elastic limit.

The result is initially surprising as the crystal packing modes are very similar (Figures 2, S9, and S10). Selected TAS-acene analogues all pack into similar 2D brickwork structures, which are directed by molecular design based on an empirical geometric model—2D brickwork structure is favored when the ratio of the diameter of TAS ellipsoid to the length of acene core is approximately 0.5.[49] As a general feature, these structures have two different π-stacking axes; the main (secondary) π-stacking aligns along the $a-b$ pair ($a-c$ pair) direction (Figure 2). However, there are also important structural differences that can cause the difference in ferroelastic transition capabilities. First, it is the centroid-to-centroid distance in the $a-d$ pair (Cg_{a-d}), which is much closer in diF-TES-ADT compared to other analogues. Second, it is fluorine-induced intermolecular interactions between $a-d$ pair that are present in the diF-TES-ADT and diF-TIPS-ADT structures but absent from TIPS-P and TIPGe-P. Third, it is pitch angle (θ_{pitch}, Figures S9 and S10a) differences among the four crystal systems. Last, it is out-of-plane intermolecular interactions between neighboring TAS side chains. As detailed below, the first two factors restrain the molecular yaw-angle (θ_{yaw}, Figures S9 and S10b) rotation, which is essential for the lattice reorientation upon FE2; the latter two most likely restrain the dynamic reconfiguration of side chains that facilitates molecular gliding and rotation during ferroelastic transitions. See Table S1 for more detailed structural characteristics.

Structural Analysis and Molecular Origin of TIPS-P Ferroelasticity. What are the major factors that determine

https://doi.org/10.1021/acs.chemmater.2c02534
Chem. Mater. 2023, 35, 81−93

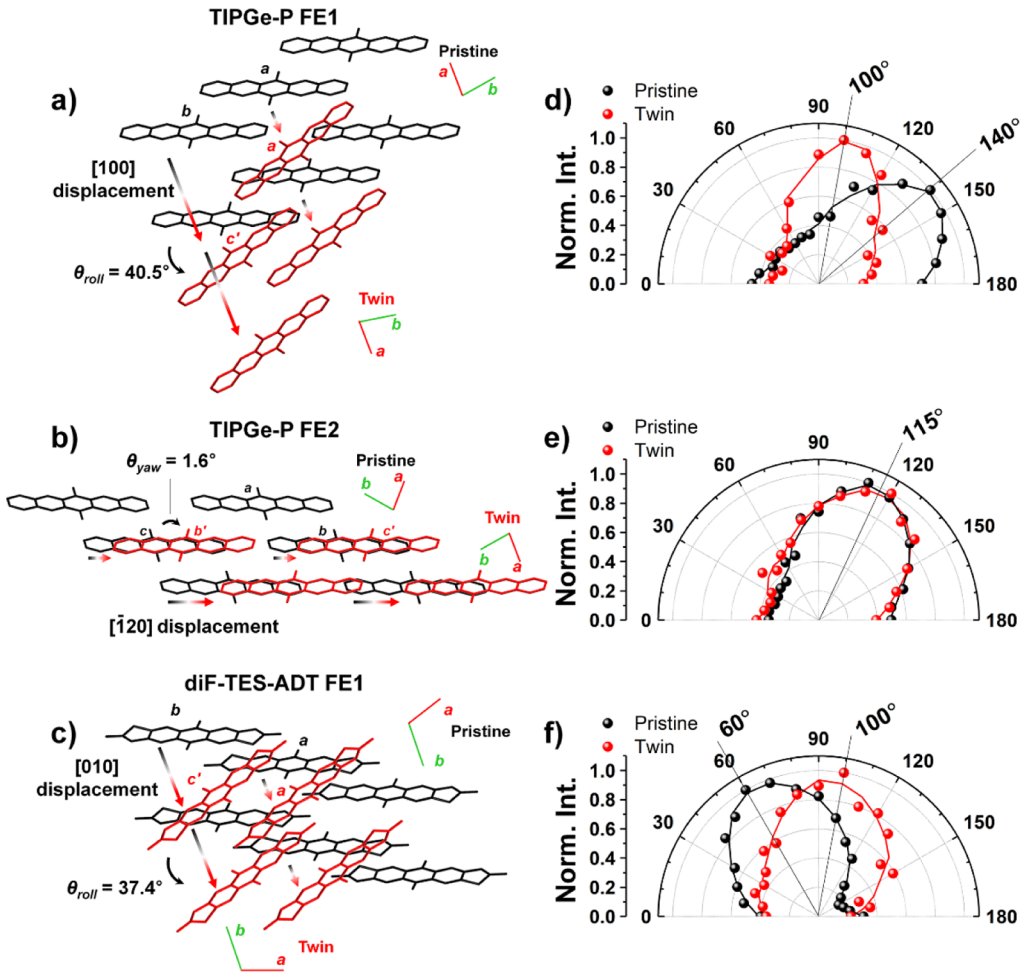

Figure 4. Description of the transformed structure by (a) FE1 of TIPGe-P, (b) FE2 of TIPGe-P, and (c) FE1 of diF-TES-ADT. Black and red molecules correspond to pristine and twinned structures, respectively. Changes in the molecular roll-angle orientations by (d) FE1 of TIPGe-P, (e) FE2 of TIPGe-P, and (f) FE1 of diF-TES-ADT, determined by polarized Raman spectroscopy. Black and red spheres correspond to normalized Raman intensities at each angle obtained from the pristine and twinned structures, respectively.

the ability of ferroelastic transition at the molecular level? To answer this question, it is necessary to decipher the molecular motions essential for ferroelastic transitions of TAS-acene crystals. Combining SC-XRD and MD simulation, we show that cooperative molecular motion and side-chain reconfiguration are essential for inducing ferroelastic transitions. Here, cooperative molecular motion comprises molecular displacement along the twinning interface, while the FE1 (FE2) transition includes cooperative molecular roll (yaw)-angle rotation. While our prior work showed the importance of cooperative molecular motion in TIPS-P by SC-XRD, MD in this work further reveals the important role of side-chain reconfiguration. Intriguingly, such molecular behaviors are further validated by comparing four TAS-acene systems.

As recently revealed,[33,34] single crystals of TIPS-P undergo FE1 transition by exerting *x*-shear. Upon FE1 transition, the lattice is reoriented by 180°-rotation against (100) twin plane normal (Figure S11a). Moreover, TIPS-P undergoes FE2 transition by exerting *y*-shear, resulting in 180°-rotation of the lattice around [2$\bar{1}$0] vector (Figure S11b). Such orientational relationships are accomplished by cooperative displacement and rotation of the molecules. As depicted in Figures 3a and S11a, FE1 transition is accompanied by substantial molecular displacement along [010] and 41.8° roll-angle (θ_{roll}) rotation. In comparison, FE2 transition is mainly accomplished by substantial molecular displacement along [2$\bar{1}$0], with small yaw-angle rotation of the molecules (2.2°, Figures 3b and S11b). Both FE1 and FE2 transitions exchange the π-stacking axes between [100] and [$\bar{1}$10], that is, $a-b$ ($a-c$) pair in the pristine domain changes into $a-c'$ ($a-b'$) pair in the twinned structure (Figure 3a,b).

Besides displacement and rotation of the molecules, MD simulation reveals that reconfiguring motions of side chains are essential to promote FE1 and FE2 transitions, which relieves the steric strain at the twinning interface. Figure 3c–f,g–j summarizes intriguing rotational motions of TIPS units during FE1 and FE2 processes, respectively. Figure 3c (3g) shows FE1 (FE2)-induced twinned structure evolution accomplished by *x*-shear (*y*-shear), where the pristine structure, intermediate interface structure, and twinned structure are color-coded by green, red, and blue, respectively. The interface structure in this case is a molecular layer discovered through simulation, which mediates the pristine and twinned domains based on neutrality in terms of molecular orientation and position.[33] In the pristine structure, before exerting mechanical stress onto the structure, TIPS units adopt the same orientation as defined by SC-XRD result (indicated by black arrows in Figure 3d,h). Meanwhile, rotation of the TIPS units is evident during FE1

https://doi.org/10.1021/acs.chemmater.2c02534
Chem. Mater. 2023, 35, 81−93

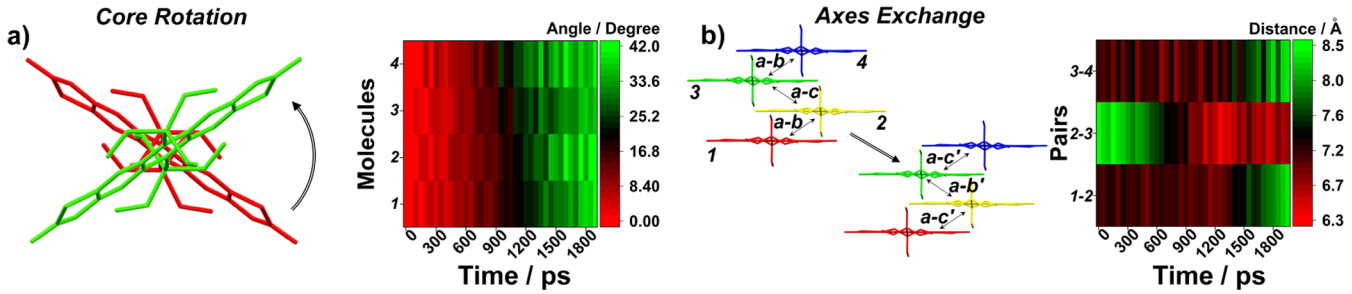

Figure 5. AIMD-simulated molecular motions upon FE1 process of diF-TES-ADT crystal. (a) Core rotation (roll angle) vs time contour plot. (b) Centroid-to-centroid distance vs time contour plot, exhibiting axes exchanging behavior (i.e., pair switching from $a-b$ to $a-c'$).

and FE2 transitions—see red arrows in Figure 3e,i denoting a new TIPS orientation in the twinned structure. In the contour plot shown in Figure 3f,j top, we represent TIPS rotational angle of molecules 1−6, which belong to six adjacent layers denoted in Figure 3c,g. Figure 3f,j bottom represents Si−Si distance between the nth and n + 1th molecules (n = 1 to 6). In Figure 3f,j top, the contour plot changes color from red to green, indicating that TIPS units rotate by 12.9 ± 2.7 and 23.2 ± 0.8° for FE1 and FE2, respectively (Figures S12 and S13). The color evolution from red to green in Figure 3f,j bottom represents that the average Si−Si distance between the nth and n + 1th molecules changes from 10.0 ± 0.0 to 8.3 ± 0.1 Å for FE1 and from 10.0 ± 0.0 to 8.0 ± 0.2 Å for FE2, respectively (Figures S12 and S13). Interestingly, in Figure 3f,j top and bottom, such color change occurs concurrently, indicating that TIPS reorientation of the nth molecule occurs as TIPS unit of the n + 1th molecule approaches toward that of the nth molecule.

We reason that such side-chain rotations occur to relieve the steric strain/stress at the twinning interface. As shown in Figure 3k, TIPS units are arranged in a specific orientation in the pristine structure without mirror symmetry. Upon exerting stress, the structure undergoes twinning; thus, the $a-b$ ($a-c$) pair becomes $a-c'$ ($a-b'$) pair by the axes switching mechanism. Due to the lack of mirror symmetry, the TIPS orientations are distinct between $a-b$ and $a-b'$ in the absence of side chain rotation, leading to strong steric crowding across the twinning interface (Figure 3l). This necessitates rotation of the side chains to relieve the steric strain at the twinning interface. Moreover, as shown in Figure S14, the conformation of side chains also changes upon transition, which will further facilitate the dynamic processes. We believe the capabilities of side-chain reconfiguration are among the primary factors determining whether TAS-acene crystals can undergo ferroelastic transitions, shown below.

Structural Analysis of Ferroelasticity in Other TAS-Acene Derivatives. As summarized in Figure 1b, the crystals of TIPGe-P are capable of FE1 and FE2 transitions, while the crystals of diF-TES-ADT exhibit FE1 transition only. In contrast, the crystals of diF-TIPS-ADT are absent from any ferroelastic transition. In order to decipher how the lattice is reoriented by the TIPGe-P and diF-TES-ADT ferroelastic transitions, we perform SC-XRD, Raman, and CPOM experiments.

SC-XRD results are summarized in Figures 4 and S4. In the case of TIPGe-P ferroelastic transitions, it follows the same principles as those of TIPS-P, which is expected due to their close structural similarity. FE1 transition of TIPGe-P is achieved by 180° rotation about the (010) plane normal with $(010)_P//(0\bar{1}0)_T$ as the twin interface. In the case of FE2 transition of TIPGe-P, the lattice reorientation is accomplished by 180° rotation about the $[\bar{1}20]$ vector with $(210)_P//(210)_T$ twinning interface. By the FE1 transition, acene cores of TIPGe-P are rotated by 40.5° at the roll angle (Figure 4a). Such a change in molecular orientation is further corroborated by polarized Raman spectroscopy (Figures 4d and S15a,b). Specifically, we measure polarized angle-dependent intensity ratio of peaks that are assigned as C−C ring stretch modes in the long- and short-axis directions of TIPGe-P molecule. For this, we analyze experimental and DFT-calculated Raman spectra (Figure S15). Based on the well-established method,[62,63] we are able to identify peaks at 1375 and 1578 cm^{-1} as stretch modes in the molecular short- and long-axis directions, although there are prevalent differences between spectra likely due to under-/overestimation of simulated peak intensity, peak merging, packing effect, and the presence of conformers (in diF-TES-ADT case).[64] The polar plot in Figure 4d represents the polarized angle-dependent intensity ratio of corresponding peaks (i.e., I_{1578}/I_{1375}), indicating that the molecular long axis is oriented in the direction of the angle where the ratio is the greatest. Therefore, we verify that the molecules are rotated by ca. 40° at the roll angle upon FE1 of TIPGe-P. On the other hand, polarized Raman spectroscopy on FE2 transformed crystals verifies that the acene cores are not subjected to roll-angle rotation (Figure 4b,e). Indeed, SC-XRD shows that there is only a small yaw-angle shift (1.6°) in the FE2 case (Figures 4b and S4). In addition to revealing lattice reorientation mechanisms, SC-XRD confirms that π-stacking axes switching occurs in both FE1 and FE2 transitions of the TIPGe-P crystals as in the case of TIPS-P. Specifically, the (100) facet of the crystal changes to $(1\bar{1}0)$ and vice versa upon transition (Figure S4). Such structural attributes are affirmed by the deformed shape of the crystals, see CPOM study in Figure S16a,b.

We also examined the structural change for diF-TES-ADT using Raman and CPOM. Due to the thinness of the crystal, SC-XRD was inaccessible. Overall, the FE1 structural transition is highly similar to the TIPS-P and TIPGe-P cases. As shown in the polarized Raman spectroscopy results (Figures 4f and S15c,d), molecular roll-angle orientation changes about 40°, like in the FE1 transition cases of the TIPS-P and TIPGe-P crystals. Moreover, measured phonon vibration spectra at both the pristine and deformed regions exhibited the same peak frequencies, suggesting that the molecular packing structure is preserved after transformation (Figure S17). Furthermore, microscopy analysis on the deformed crystals shows that characteristic angles γ and ω match well with the crystallographic angles (100)∠(010) and (100)∠ ($\bar{1}$10),

https://doi.org/10.1021/acs.chemmater.2c02534
Chem. Mater. 2023, 35, 81−93

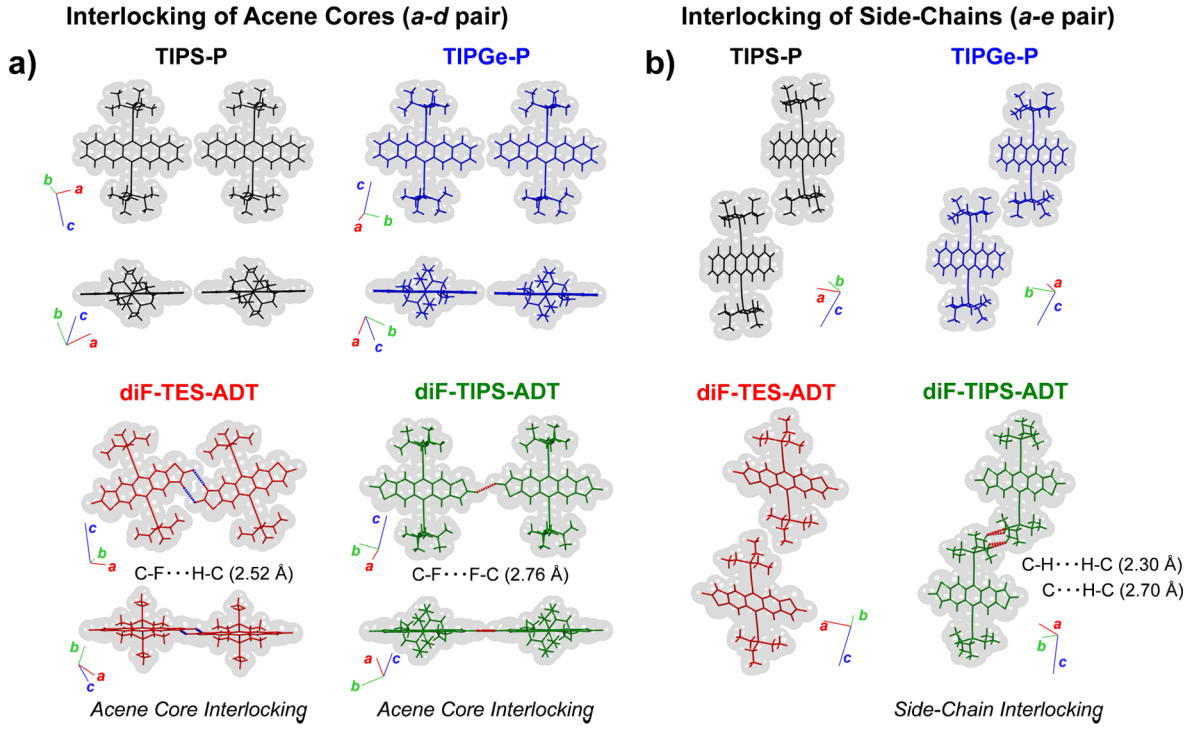

Figure 6. (a) Space-fill representations describing interlocking of acene core. (a) In the cases of TIPS-P and TIPGe-P structures, no spatial overlap in the *a*−*d* pair is found. However, diF-TES-ADT (diF-TIPS-ADT) exhibits a significant (slight) spatial overlap. Such overlap also appears as short contacts based on C−F···H−C for diF-TES-ADT and C−F···F−C for diF-TIPS-ADT. (b) Space-fill representations describing interlocking of side chains. Unlike other structures, in the case of diF-TIPS-ADT, spatial overlap in the *a*−*e* pair is prominent, which also appears as C−F···F−C and C···H−C short contacts.

respectively (Figure S16c). The result indicates that the twinning interface is (100) and the side facet changes from (010) to ($\bar{1}$10), which suggests that axes exchange mechanism also occurs in FE1 of diF-TES-ADT. Inferred structural change upon transformation is depicted in Figure 4c.

Molecular Origin of Ferroelastic Transformability of TAS-Acene Derivatives. Above, we presented structural analysis which elucidates how the lattice is reoriented by ferroelastic transition and whether the structure is preserved by the process. Next, we perform ab initio molecular dynamics (AIMD) simulations to elucidate whether the cooperative molecular motions (i.e., molecular gliding and core rotation) and the reconfiguring side-chain motions take place during lattice reorientation or fracturing of the crystal. The simulation results also unravel the reason why diF-TES-ADT does not show FE2 transition and diF-TIPS-ADT does not show FE1 and FE2 transitions. Given that the ferroelastic behavior of TIPGe-P is almost identical to TIPS-P, we did not perform further simulations on TIPGe-P.

In AIMD simulations on diF-TES-ADT and diF-TIPS-ADT structures, we exert *x*-shear for FE1 and tensile loading (thus, *y*-shear) for FE2, respectively. As shown in Figures 5a and S18, by exerting *x*-shear onto 2 × 2 × 1 super-cell of diF-TES-ADT structure, molecules exhibit about 40° roll-angle rotation [color evolution from red (0°) to green (40°)]. More interestingly, the AIMD properly reflects the axes exchange behavior upon FE1 of diF-TES-ADT. As depicted in Figure 5b, in the twinned structure of 2D brickwork TAS-acene crystals, main π-stacking axis pairs (*a*−*b*) become secondary π-stacking axis pairs (*a*−*c*′) and vice versa. In the diF-TES-ADT case, such behavior should induce centroid-to-centroid distance evolution from 7.10 to 8.46 Å and 8.46 to 7.10 Å for *a*−*b* and *a*−*c* pair, respectively. The contour plot in Figure 5b manifests color evolution from red to green for 1−2 and 3−4 pairs (*a*−*b* in the pristine structure) and from green to red for 2−3 pair (*a*−*c* in the pristine structure), representing axes exchange behavior. Such structural alterations (i.e., roll-angle rotation and axes exchange) corroborate twinnability of diF-TES-ADT structure upon exerting *x*-shear, which are consistent with the polarized Raman and CPOM results (Figures 4f and S16c).

Furthermore, we investigate the reconfiguring side-chain motions upon FE1 of diF-TES-ADT based on the AIMD simulation result. As shown in Figures S19a−c, seven TES units rotate about −4.5 ± 17.3° in average, which is characterized by measuring the dihedral angle between the plane parallel to the acene core and the plane consisting of the side-chain axle and one of the ethyl branches. Such slight side-chain rotations possibly take place to reduce steric strain incurred during twinning transition. Meanwhile, one of the eight TES units (molecule 2, top) is shown to represent a significant rotation (−66.6°), which is most likely due to stabilization of the dynamic structure resulted from structural transition by minimizing steric crowding. These molecular motions are slightly different from the reconfiguring side-chain motions of TIPS-P, which shows well-aligned TIPS orientation even after transition. Nonetheless, consistent with the TIPS-P case, the simulated FE1 of diF-TES-ADT suggests that the TES side chains rotate to mechanically adapt the ferroelastic transition. Upon transition, moreover, a considerable torsional twisting can simultaneously occur in the ethyl branches to further mitigate steric strain caused by neighboring rotator side chains (Figure S19d−f). Although the model size in AIMD simulation is rather limited to present precise statistical analyses on side-chain motions, the observation signifies how

https://doi.org/10.1021/acs.chemmater.2c02534
Chem. Mater. 2023, 35, 81−93

important the reconfiguration behaviors of side chains are for the ferroelastic transition, as in the case of TIPS-P crystal (Figure 3). However, it should be mentioned that the model system will not be a perfect representation of a real system; for instance, we speculate that the outlier rotational angle (e.g., −66.6°) would not always occur but will result in varying angles of side-chain rotation and torsional twisting.

Unlike the *x*-shearing case of diF-TES-ADT structure, it was verified through AIMD simulation that the tensile loading (thus *y*-shear) onto the diF-TES-ADT structure or the *x*-shear/tensile loading onto the diF-TIPS-ADT structure could not keep the structure intact. As can be seen in Figure S20, axes exchange behavior—that is, color evolution from green to red and vice versa—does not appear in these cases. In addition, inequivalent pitch, yaw, and roll angles in constituting molecules imply that the crystal can undergo fracturing process by the corresponding mechanical stress (Figure S21). The simulation result is consistent with experimental observations (Figures 1b and S8).

Why the tensile loading (i.e., *y*-shear) onto the diF-TES-ADT crystal or the *x*-shear/tensile loading onto the diF-TIPS-ADT crystal does not lead to ferroelastic transition? Further structural analysis detailed below suggests that the absence of FE2 from the diF-TES-ADT structure is due to interlocking of acene cores in the molecular π-plane, while the absence of FE1 and FE2 from the diF-TIPS-ADT structure is mainly due to interlocking of side chains.

As revealed above, FE2 transition is accompanied by 180° rotation of lattice about the vector parallel to acene unit alignment direction (i.e., $[2\bar{1}0]$ and $[\bar{1}20]$ for TIPS-P and TIPGe-P, respectively), which gives rise to the yaw-angle tilting. In the cases of TIPS-P and TIPGe-P crystals, due to the small yaw angle in the pristine lattice (TIPS-P: 1.1° and TIPGe-P: 0.8°), FE2 transition of TIPS-P and TIPGe-P only requires a yaw-angle tilting of 2.2 and 1.6°, respectively. Upon transition, steric crowding between *a*−*d* pair is expected to be low, attributed to the large Cg_{a-d} distance (TIPS-P: 16.35 Å; TIPGe-P: 16.33 Å, Figure 2). However, as shown in Figure 2, diF-TES-ADT structure exhibits a much closer Cg_{a-d} distance (13.88 Å) than others, which is shorter than the molecular length measured along the core direction (14.37 Å). This indicates that the neighboring acene cores are interlocked in the molecular π-plane of diF-TES-ADT. The core interlocking is achieved by noticeable yaw-angle molecular tilting (20.3°, Figure S10b), which allows the molecules of the *a*−*d* pair to get closer. As shown by the space-fill representation of the molecular packing (Figure 6a), diF-TES-ADT molecules in *a*−*d* pairs are closely interlocked, while other crystals show negligible core interlocking. Moreover, as illustrated in Figure 6a, diF-TES-ADT exhibits short contact based on C−F···H−C interactions. Such a core interlocking leads to the absence of FE2 transition in the diF-TES-ADT crystals. As described above, FE2 transitions of TIPS-P and TIPGe-P are accomplished by the molecular rotations at the yaw angle, that is, 2.2 and 1.6° by $2 \times \theta_{yaw}$. Since the molecular rotation and the core interlocking are negligible in these cases, the corresponding molecular motion is not sterically demanding. On the contrary, the situation becomes very different in the diF-TES-ADT case. Given that ferroelasticity is a layer-by-layer process, concerted motion of molecules should occur within each layer. In the FE2 of TAS acenes, molecules in the a−d relationship belong to the same layer; therefore, for FE2 of diF-TES-ADT, these molecules should undergo 40.6° yaw-angle rotation at the same time. As illustrated in Figure S22, such molecular motion will cause a collision between the cores in the *a*−*d* pair. In addition, it appears that the dynamic molecular rotation/displacement should be further restricted by C−F···H−C interactions. Therefore, we surmise that the frustration of FE2 transition in diF-TES-ADT is primarily caused by the core interlocking-induced steric hindrance and auxiliary by the supramolecular synthon (C−F···H−C).

The diF-TIPS-ADT structure, on the other hand, represents molecular packing similar to TIPS-P and TIPGe-P (Figure 2, Table S1). Despite structural similarity, we notice that strong interlocking of side chains precludes ferroelastic transitions in diF-TIPS-ADT. As presented in Figure 6b, interlocking of the side chain is nontrivial in all TAS-acene derivatives due to the pitch angles in the packing structures (60.7−77.1°, see Table S1 and Figure S10). However, interlocking of the side chain between the nearest out-of-plane molecular pair (i.e., *a*−*e*) is much more prominent in the diF-TIPS-ADT case due to the smallest pitch angle in the diF-TIPS-ADT crystal structure (60.7°). Moreover, as shown in Figure 6b, TIPS units of diF-TIPS-ADT exhibit short contact based on C−H···H−C and C···H−C, which supports the inference of stronger side-chain interactions. Such an interlocking of side chains along both in-plane and out-of-plane directions restricts facile reconfiguring motions of the side chain, thereby hindering the ferroelastic transition.

As pointed out above, the reconfiguring side-chain motions are accompanied by both FE1 and FE2 transitions of TAS acenes. The corresponding molecular motions are imperative to mitigate the stress caused by the spatial overlap of adjacent side chains at the transition interface. Specifically, they are rotation and torsional twisting of the side chain to reduce the stress or steric strain induced by creating intralayer *a*−*c*′ pair from *a*−*b* pair. In the case of TIPS-P, TIPGe-P, and diF-TES-ADT crystals, such motions will be unhindered by negligibly weak interlayer interactions. On the contrary, diF-TIPS-ADT has considerable interactions in the *a*−*e* pair; hence, side chains in the interlayer molecules prevent the side-chain rotation. In this respect, interfacial stress cannot be easily dissipated, leading to brittle fracture of diF-TIPS-ADT crystals when mechanical stress is exerted. In addition, the C−F···F−C interaction in *a*−*d* pair (Figure 6a) may also frustrate the FE2 transition in diF-TIPS-ADT crystals by hampering cooperative yaw-angle rotation of the molecules.

Molecular and Crystal Design Perspectives for Ferroelasticity in 2D Brickwork Packing TAS-Acenes. The molecular and crystal design perspectives for devising deformable 2D brickwork packing TAS acenes through ferroelasticity are summarized below. These materials possess important structural features that enable ferroelastic transitions: (i) the establishment of coplanar π-planes for a facile cooperative displacement of molecules, (ii) the formation of colinear rotational axes for roll- and yaw-angle rotations, and (iii) the incorporation of reconfigurable side chains that can adapt to the dynamic structure induced upon lattice reorientation.[46] In principle, these attributes are consolidated into the 2D brickwork structures that are designed by the empirical geometrical model of Anthony and colleagues.[48−50] They are also the result of strategic supramolecular design—for example, the emergence of $\pi\cdots\pi$ supramolecular synthons by introducing bulky side chains, and the formation of CF···HC or CF···FC synthons by introducing fluorine atoms. Therefore, it is deciphered that the 2D brickwork pattern and

https://doi.org/10.1021/acs.chemmater.2c02534
Chem. Mater. 2023, 35, 81−93

accompanying attributes are driven by the unique geometry of the molecules (shape and steric factors) and induced supramolecular synthons. However, despite having all the attributes (i−iii), it is revealed that not all of the analogues exhibit ferroelastic transition. Our findings suggest that in order to facilitate ferroelasticity, it should be taken into account how well the molecules adapt to dynamic structures beyond static ones. Specifically, the excellent adaptability among these analogues is demonstrated when they are free from core-/side-chain interlocking and short contacts between neighboring molecules. Therefore, we believe that the following criteria should be carefully dealt with for the further development of deformable 2D brickwork packing TAS acenes.

Particular attention is required in substituting both ends of the acene core. Incorporation of functional units at these positions can lead to $a-d$ pair interactions, thus inducing geometrical constraints for yaw-angle rotation, that is, core interlocking (e.g., diF-TES-ADT). It should also be considered that the supramolecular synthon itself may prevent or resist the cooperative molecular motions. For instance, close contact formation (i.e., interatomic distance less than the sum of the van der Waals radii) by establishing supramolecular synthon also gives rise to steric crowding that prevents dynamic motions of molecules. Moreover, strong intermolecular interactions between functional units can resist molecular motions in response to mechanical loading. Such characteristics are reflected in diF-TES-ADT and diF-TIPS-ADT structures, while cooperative roll-angle rotation achieved in the former case is most likely due to the direction of molecular rotation being nearly orthogonal to the contact direction and the weak interaction energy of CF···HC.[65,66] To further understand the impact of $a-d$ pair interactions, however, experimental and theoretical evaluations of energetic costs for ferroelastic transitions are required using a series of isostructural TAS acenes with different supramolecular synthons. Similarly, the effect of the $\pi-\pi$ interaction strength on ferroelasticity is worth evaluating because the substitution can fortify $\pi-\pi$ interactions by increased electrostatic energy, charge penetration effects, or direct interactions between the substituent and π-system based on dispersion energy.[67−69]

The choice of side chain is as important as the design of the acene units. The size and shape of the side chains in TAS acenes significantly contribute to the molecular arrangement. For instance, pentacene functionalized with TIPS and TES side chains exhibit 2D brickwork packing and slipped π-stacking, respectively. Since the shape of TES is less spherical than TIPS, there is increased free volume surrounding this unit. As a result, π-stacking molecules in TES-P can come closer (7.20 Å) based on a yaw-angle tilting of 13.1° for close packing, which is very different from the molecular arrangement of TIPS-P (Cg_{a-b}: 7.74 Å, θ_{yaw}: 1.1°).[70] Intriguingly, both diF-TES-ADT and diF-TIPS-ADT show similar molecular arrangements to their pentacene counterparts. Specifically, diF-TES-ADT shows a short Cg_{a-b} of 7.10 Å and a large θ_{yaw} of 20.3°, while diF-TIPS-ADT shows a long Cg_{a-b} of 8.10 Å and a small θ_{yaw} of 0.2°. However, instead of slipped π-stacking, diF-TES-ADT adopts 2D brickwork packing with core interlocking most likely due to the formation of multiple CF···HC synthons between $a-d$ pair. The result indicates that the introduction of a less spherical side chain (e.g., TES) causes core interlocking due to excessive yaw-angle tilting of the molecules, thus preventing FE2 transition. Meanwhile, once the molecular arrangements are isostructural, it is discovered that a small (2%) increase in side-chain bulkiness by replacing silicon atoms in TIPS-P with germanium (TIPGe-P) has a minor impact on the ferroelastic transition capability.[51] However, we surmise that there is difference in energy to accomplish ferroelastic transition, which can be confirmed by the difference in thermoelastic transition temperatures between these materials (Movies S4 and S5). To gain further insight, it is a subject worth pursuing in the future to compare energetic costs for ferroelastic transitions on both silicone- and germanium-containing TAS-acene derivatives.

CONCLUSIONS

In this study, the generality and mechanism of ferroelastic transitions of 2D brickwork packing TAS-acene derivatives are elucidated. From the structural aspect, twinning is accomplished by π-stacking axes exchange mechanism, which is facilitated by cooperative molecular displacement along uniaxially aligned π-plane in response to mechanical shear or tensile loading. In addition to the axes exchange mechanism, the ferroelastic transitions in these crystals are accompanied by (1) cooperative acene core rotation and (2) reconfiguration of side chains. The former molecular motion is to achieve twin correlation between the pristine and deformed lattices, while the latter motion is in charge of relieving steric strain occurring upon the transition. In order to represent such molecular motions, we reveal that interlocking of acene core/side chain should be avoided and reduce steric strain. Through this study, we not only signify that the organic semiconductor with 2D brickwork structure can become a new class of semiconductor showing intrinsic flexibility through cooperative transition but also reveal important crystal design rule to enable corresponding transitions.

ASSOCIATED CONTENT

Supporting Information

The Supporting Information is available free of charge at https://pubs.acs.org/doi/10.1021/acs.chemmater.2c02534.

Additional polarized optical micrographs, SC-XRD result on twinned TIPGe-P, (polarized) Raman spectra, DFT-calculated Raman spectra, and MD/AIMD simulation results (PDF)

Pushing TIPS-P crystals on SiO_2 with nylon wire at room temperature (MP4)

Pushing TIPS-P crystals on SiO_2 with nylon wire at 150 °C(MP4)

Thickness dependence of ferroelasticity of TIPS-P by thermal annealing (MP4)

Heating−cooling TIPGe-P on SiO_2 (MP4)

Heating−cooling TIPS-P on SiO_2 (MP4)

AUTHOR INFORMATION

Corresponding Authors

Sang Kyu Park − *Department of Chemical and Biomolecular Engineering, University of Illinois Urbana—Champaign, Urbana, Illinois 61801, United States; Functional Composite Materials Research Center, Institute of Advanced Composite Materials, Korea Institute of Science and Technology, Wanju-gun, Joellabuk-do 55324, Republic of Korea;* orcid.org/0000-0002-1184-7720; Email: skpark86@kist.re.kr

Kejie Zhao − *School of Mechanical Engineering, Purdue University, West Lafayette, Indiana 47907, United States;*

https://doi.org/10.1021/acs.chemmater.2c02534
Chem. Mater. 2023, 35, 81−93

orcid.org/0000-0001-5030-7412; Email: kjzhao@purdue.edu

Ying Diao − *Department of Chemical and Biomolecular Engineering, University of Illinois Urbana—Champaign, Urbana, Illinois 61801, United States;* orcid.org/0000-0002-8984-0051; Email: yingdiao@illinois.edu

Authors

Hong Sun − *School of Mechanical Engineering, Purdue University, West Lafayette, Indiana 47907, United States; Physics Division, Lawrence Livermore National Laboratory, Livermore, California 94550, United States*

Michael Bernhardt − *Department of Chemical and Biomolecular Engineering, University of Illinois Urbana—Champaign, Urbana, Illinois 61801, United States*

Kyoungtae Hwang − *Functional Composite Materials Research Center, Institute of Advanced Composite Materials, Korea Institute of Science and Technology, Wanju-gun, Joellabuk-do 55324, Republic of Korea*

John E. Anthony − *Department of Chemistry & Center for Applied Energy Research, University of Kentucky, Lexington, Kentucky 40506-0055, United States;* orcid.org/0000-0002-8972-1888

Complete contact information is available at: https://pubs.acs.org/10.1021/acs.chemmater.2c02534

Author Contributions

#S.K.P. and H.S. contributed equally to this work.

Notes

The authors declare no competing financial interest.

■ ACKNOWLEDGMENTS

Y.D. acknowledges the Sloan Foundation for a Sloan Research Fellowship in Chemistry and a 3M Nontenured Faculty Award. H.S. and K.Z. acknowledge the support from the National Science Foundation through grant CMMI-1941323. S.K.P. acknowledges the Basic Science Research Program through the National Research Foundation of Korea (NRF) funded by the Ministry of Education (2022R1C1C1005241) and the Korea Institute of Science and Technology (KIST) Institutional Program. J.E.A. acknowledges support from the National Science Foundation DMREF program, DMR-1627428. This work was conducted in part in the Frederick Seitz Materials Research Laboratory Central Facilities and at the Beckman Institute for Advanced Science and Technology at UIUC.

■ REFERENCES

(1) Buehler, W. J.; Wang, F. E. A summary of recent research on the nitinol alloys and their potential application in ocean engineering. *Ocean Eng.* **1968**, *1*, 105−120.

(2) Wei, Z.; Sandström, R.; Mlyazaki, S. Review shape-memory materials and hybrid composites for smart systems. *J. Mater. Sci.* **1998**, *33*, 743.

(3) Otsuka, K.; Wayman, C. M.*Shape Memory Materials*; Cambridge University Press: Cambridge, 1999.

(4) Otsuka, K.; Ren, X. Physical metallurgy of Ti-Ni-based shape memory alloys. *Prog. Mater. Sci.* **2005**, *50*, 511−678.

(5) Mohd Jani, J.; Leary, M.; Subic, A.; Gibson, M. A. A review of shape memory alloy research, applications and opportunities. *Mater. Des.* **2014**, *56*, 1078−1113.

(6) Skoko, Ž.; Zamir, S.; Naumov, P.; Bernstein, J. The Thermosalient Phenomenon. "Jumping Crystals" and Crystal Chemistry of the Anticholinergic Agent Oxitropium Bromide. *J. Am. Chem. Soc.* **2010**, *132*, 14191−14202.

(7) Sahoo, S. C.; Sinha, S. B.; Kiran, M. S.; Ramamurty, U.; Dericioglu, A. F.; Reddy, C. M.; Naumov, P. Kinematic and mechanical profile of the self-actuation of thermosalient crystal twins of 1,2,4,5-tetrabromobenzene: a molecular crystalline analogue of a bimetallic strip. *J. Am. Chem. Soc.* **2013**, *135*, 13843−13850.

(8) Panda, M. K.; Runčevski, T.; Chandra Sahoo, S. C.; Belik, A. A.; Nath, N. K.; Dinnebier, R. E.; Naumov, P. Colossal positive and negative thermal expansion and thermosalient effect in a pentamorphic organometallic martensite. *Nat. Commun.* **2014**, *5*, 4811.

(9) Panda, M. K.; Runčevski, T.; Husain, A.; Dinnebier, R. E.; Naumov, P. Perpetually self-propelling chiral single crystals. *J. Am. Chem. Soc.* **2015**, *137*, 1895−1902.

(10) Karothu, D. P.; Weston, J.; Desta, I. T.; Naumov, P. Shape-Memory and Self-Healing Effects in Mechanosalient Molecular Crystals. *J. Am. Chem. Soc.* **2016**, *138*, 13298−13306.

(11) Panda, M. K.; Etter, M.; Dinnebier, R. E.; Naumov, P. Acoustic Emission from Organic Martensites. *Angew. Chem., Int. Ed.* **2017**, *56*, 8104−8109.

(12) Gupta, P.; Karothu, D. P.; Ahmed, E.; Naumov, P.; Nath, N. K. Thermally Twistable, Photobendable, Elastically Deformable, and Self-Healable Soft Crystals. *Angew. Chem., Int. Ed.* **2018**, *57*, 8498−8502.

(13) Tamboli, M. I.; Karothu, D. P.; Shashidhar, M. S.; Gonnade, R. G.; Naumov, P. Effect of Crystal Packing on the Thermosalient Effect of the Pincer-Type Diester Naphthalene-2,3-diyl-bis(4-fluorobenzoate): A New Class II Thermosalient Solid. *Chem.—Eur. J.* **2018**, *24*, 4133−4139.

(14) Colin-Molina, A.; Karothu, D. P.; Jellen, M. J.; Toscano, R. A.; Garcia-Garibay, M. A.; Naumov, P.; Rodríguez-Molina, B. Thermosalient Amphidynamic Molecular Machines: Motion at the Molecular and Macroscopic Scales. *Matter* **2019**, *1*, 1033−1046.

(15) Khalil, A.; Karothu, D. P.; Naumov, P. Direct Quantification of Rapid and Efficient Single-Stroke Actuation by a Martensitic Transition in a Thermosalient Crystal. *J. Am. Chem. Soc.* **2019**, *141*, 3371−3375.

(16) Li, L.; Commins, P.; Al-Handawi, M. B.; Karothu, D. P.; Halabi, J. M.; Schramm, S.; Weston, J.; Rezgui, R.; Naumov, P. Martensitic organic crystals as soft actuators. *Chem. Sci.* **2019**, *10*, 7327−7332.

(17) Ahmed, E.; Karothu, D. P.; Warren, M.; Naumov, P. Shape-memory effects in molecular crystals. *Nat. Commun.* **2019**, *10*, 3723.

(18) Takamizawa, S.; Miyamoto, Y. Superelastic organic crystals. *Angew. Chem., Int. Ed.* **2014**, *53*, 6970−6973.

(19) Takamizawa, S.; Takasaki, Y. Shape-memory effect in an organosuperelastic crystal. *Chem. Sci.* **2016**, *7*, 1527−1534.

(20) Takamizawa, S.; Takasaki, Y. Versatile Shape Recoverability of Odd-Numbered Saturated Long-Chain Fatty Acid Crystals. *Cryst. Growth Des.* **2019**, *19*, 1912−1920.

(21) Mutai, T.; Sasaki, T.; Sakamoto, S.; Yoshikawa, I.; Houjou, H.; Takamizawa, S. A superelastochromic crystal. *Nat. Commun.* **2020**, *11*, 1824.

(22) Sakamoto, S.; Sasaki, T.; Sato-Tomita, A.; Takamizawa, S. Shape Rememorization of an Organosuperelastic Crystal through Superelasticity-Ferroelasticity Interconversion. *Angew. Chem., Int. Ed.* **2019**, *58*, 13722−13726.

(23) Takasaki, Y.; Takamizawa, S. Active porous transition towards spatiotemporal control of molecular flow in a crystal membrane. *Nat. Commun.* **2015**, *6*, 8934.

(24) Takamizawa, S.; Takasaki, Y. Superelastic shape recovery of mechanically twinned 3,5-difluorobenzoic acid crystals. *Angew. Chem., Int. Ed.* **2015**, *54*, 4815−4817.

(25) Takamizawa, S.; Takasaki, Y.; Sasaki, T.; Ozaki, N. Superplasticity in an organic crystal. *Nat. Commun.* **2018**, *9*, 3984.

(26) Mir, S. H.; Takasaki, Y.; Engel, E. R.; Takamizawa, S. Ferroelasticity in an Organic Crystal: A Macroscopic and Molecular Level Study. *Angew. Chem., Int. Ed.* **2017**, *56*, 15882−15885.

(27) Engel, E. R.; Takamizawa, S. Versatile Ferroelastic Deformability in an Organic Single Crystal by Twinning about a Molecular Zone Axis. *Angew. Chem., Int. Ed.* **2018**, *57*, 11888−11892.

(28) Chung, H.; Diao, Y. Polymorphism as an emerging design strategy for high performance organic electronics. *J. Mater. Chem. C* **2016**, *4*, 3915−3933.
(29) Chung, H.; Dudenko, D.; Zhang, F.; D'Avino, G.; Ruzié, C.; Richard, A.; Schweicher, G.; Cornil, J.; Beljonne, D.; Geerts, Y.; et al. Rotator side chains trigger cooperative transition for shape and function memory effect in organic semiconductors. *Nat. Commun.* **2018**, *9*, 278.
(30) Chung, H.; Chen, S.; Sengar, N.; Davies, D. W.; Garbay, G.; Geerts, Y. H.; Clancy, P.; Diao, Y. Single Atom Substitution Alters the Polymorphic Transition Mechanism in Organic Electronic Crystals. *Chem. Mater.* **2019**, *31*, 9115−9126.
(31) Chung, H.; Ruzié, C.; Geerts, Y.; Diao, Y. Hybrid Mechanism of Nucleation and Cooperative Propagation in a Single-Crystal-to-Single-Crystal Transition of a Molecular Crystal. *Cryst. Growth Des.* **2018**, *18*, 4245−4251.
(32) Chung, H.; Chen, S.; Patel, B.; Garbay, G.; Geerts, Y. H.; Diao, Y. Understanding the Role of Bulky Side Chains on Polymorphism of BTBT-Based Organic Semiconductors. *Cryst. Growth Des.* **2020**, *20*, 1646−1654.
(33) Park, S. K.; Sun, H.; Chung, H.; Patel, B. B.; Zhang, F.; Davies, D. W.; Woods, T. J.; Zhao, K.; Diao, Y. Super- and Ferroelastic Organic Semiconductors for Ultraflexible Single-Crystal Electronics. *Angew. Chem., Int. Ed.* **2020**, *59*, 13004−13012.
(34) Sun, H.; Park, S. K.; Diao, Y.; Kvam, E. P.; Zhao, K. Molecular Mechanisms of Superelasticity and Ferroelasticity in Organic Semiconductor Crystals. *Chem. Mater.* **2021**, *33*, 1883−1892.
(35) Yao, Z. S.; Mito, M.; Kamachi, T.; Shiota, Y.; Yoshizawa, K.; Azuma, N.; Miyazaki, Y.; Takahashi, K.; Zhang, K.; Nakanishi, T.; et al. Molecular motor-driven abrupt anisotropic shape change in a single crystal of a Ni complex. *Nat. Chem.* **2014**, *6*, 1079−1083.
(36) Su, S. Q.; Kamachi, T.; Yao, Z. S.; Huang, Y. G.; Shiota, Y.; Yoshizawa, K.; Azuma, N.; Miyazaki, Y.; Nakano, M.; Maruta, G.; et al. Assembling an alkyl rotor to access abrupt and reversible crystalline deformation of a cobalt(II) complex. *Nat. Commun.* **2015**, *6*, 8810.
(37) Zahn, D.; Anwar, J. Collective displacements in a molecular crystal polymorphic transformation. *RSC Adv.* **2013**, *3*, 12810−12815.
(38) Anwar, J.; Tuble, S. C.; Kendrick, J. Concerted molecular displacements in a thermally-induced solid-state transformation in crystals of DL-norleucine. *J. Am. Chem. Soc.* **2007**, *129*, 2542−2547.
(39) Smets, M. M. H.; Pitak, M. B.; Cadden, J.; Kip, V. R.; de Wijs, G. A.; van Eck, E. R. H.; Tinnemans, P.; Meekes, H.; Vlieg, E.; Coles, S. J.; et al. The Rich Solid-State Phase Behavior of dl-Aminoheptanoic Acid: Five Polymorphic Forms and Their Phase Transitions. *Cryst. Growth Des.* **2018**, *18*, 242−252.
(40) Borbone, F.; Tuzi, A.; Carella, A.; Marabello, D.; Oscurato, S. L.; Lettieri, S.; Maddalena, P.; Centore, R. High-Temperature Reversible Martensitic Transition in an Excited-State Intramolecular Proton Transfer Fluorophore. *Cryst. Growth Des.* **2019**, *19*, 6519−6526.
(41) Brandel, C.; Cartigny, Y.; Couvrat, N.; Eusébio, M. E. S.; Canotilho, J.; Petit, S.; Coquerel, G. Mechanisms of Reversible Phase Transitions in Molecular Crystals: Case of Ciclopirox. *Chem. Mater.* **2015**, *27*, 6360−6373.
(42) Simões, R. G.; Bernardes, C. E. S.; Joseph, A.; M. Piedade, M. P.; Kraus, W.; Emmerling, F.; Diogo, H. P.; Minas da Piedade, M. E. Polymorphism in Simvastatin: Twinning, Disorder, and Enantiotropic Phase Transitions. *Mol. Pharmaceutics* **2018**, *15*, 5349−5360.
(43) Naumov, P.; Chizhik, S.; Panda, M. K.; Nath, N. K.; Boldyreva, E. Mechanically Responsive Molecular Crystals. *Chem. Rev.* **2015**, *115*, 12440−12490.
(44) Ahmed, E.; Karothu, D. P.; Naumov, P. Crystal Adaptronics: Mechanically Reconfigurable Elastic and Superelastic Molecular Crystals. *Angew. Chem., Int. Ed.* **2018**, *57*, 8837−8846.
(45) Naumov, P.; Karothu, D. P.; Ahmed, E.; Catalano, L.; Commins, P.; Mahmoud Halabi, J.; Al-Handawi, M. B.; Li, L. The Rise of the Dynamic Crystals. *J. Am. Chem. Soc.* **2020**, *142*, 13256−13272.
(46) Park, S. K.; Diao, Y. Martensitic Transition in Molecular Crystals for Dynamic Functional Materials. *Chem. Soc. Rev.* **2020**, *49*, 8287−8314.
(47) Seki, T.; Feng, C.; Kashiyama, K.; Sakamoto, S.; Takasaki, Y.; Sasaki, T.; Takamizawa, S.; Ito, H. Photoluminescent Ferroelastic Molecular Crystals. *Angew. Chem., Int. Ed.* **2020**, *59*, 8839−8843.
(48) Anthony, J. E. Functionalized Acenes and Heteroacenes for Organic Electronics. *Chem. Rev.* **2006**, *106*, 5028−5048.
(49) Anthony, J. E. The Larger Acenes: Versatile Organic Semiconductors. *Angew. Chem., Int. Ed.* **2008**, *47*, 452−483.
(50) Thorley, K. J.; Finn, T. W.; Jarolimek, K.; Anthony, J. E.; Risko, C. Theory-Driven Insight into the Crystal Packing of Trialkylsilylethynyl Pentacenes. *Chem. Mater.* **2017**, *29*, 2502−2512.
(51) Sorli, J. C.; Ai, Q.; Granger, D. B.; Gu, K.; Parkin, S.; Jarolimek, K.; Telesz, N.; Anthony, J. E.; Risko, C.; Loo, Y.-L. Impact of Atomistic Substitution on Thin-Film Structure and Charge Transport in a Germanyl-ethynyl Functionalized Pentacene. *Chem. Mater.* **2019**, *31*, 6615−6623.
(52) Subramanian, S.; Park, S. K.; Parkin, S. R.; Podzorov, V.; Jackson, T. N.; Anthony, J. E. Chromophore Fluorination Enhances Crystallization and Stability of Soluble Anthradithiophene Semiconductors. *J. Am. Chem. Soc.* **2008**, *130*, 2706−2707.
(53) Hutter, J.; Iannuzzi, M.; Schiffmann, F.; VandeVondele, J. cp2k: atomistic simulations of condensed matter systems. *Wiley Interdiscip. Rev.: Comput. Mol. Sci.* **2014**, *4*, 15−25.
(54) VandeVondele, J.; Hutter, J. Gaussian basis sets for accurate calculations on molecular systems in gas and condensed phases. *J. Chem. Phys.* **2007**, *127*, 114105.
(55) VandeVondele, J.; Krack, M.; Mohamed, F.; Parrinello, M.; Chassaing, T.; Hutter, J. Quickstep: Fast and accurate density functional calculations using a mixed Gaussian and plane waves approach. *Comput. Phys. Commun.* **2005**, *167*, 103−128.
(56) Krack, M. Pseudopotentials for H to Kr optimized for gradient-corrected exchange-correlation functionals. *Theor. Chem. Acc.* **2005**, *114*, 145−152.
(57) Grimme, S.; Antony, J.; Ehrlich, S.; Krieg, H. A consistent and accurate ab initio parametrization of density functional dispersion correction (DFT-D) for the 94 elements H-Pu. *J. Chem. Phys.* **2010**, *132*, 154104.
(58) Perdew, J. P.; Burke, K.; Ernzerhof, M. Generalized gradient approximation made simple. *Phys. Rev. Lett.* **1996**, *77*, 3865−3868.
(59) Briseno, A. L.; Tseng, R. J.; Ling, M.-M.; Falcao, E. H. L.; Yang, Y.; Wudl, F.; Bao, Z. High-Performance Organic Single-Crystal Transistors on Flexible Substrates. *Adv. Mater.* **2006**, *18*, 2320−2324.
(60) Park, S. K.; Kim, J. H.; Ohto, T.; Yamada, R.; Jones, A. O. F.; Whang, D. R.; Cho, I.; Oh, S.; Hong, S. H.; Kwon, J. E.; et al. Highly Luminescent 2D-Type Slab Crystals Based on a Molecular Charge-Transfer Complex as Promising Organic Light-Emitting Transistor Materials. *Adv. Mater.* **2017**, *29*, 1701346.
(61) Cui, N.; Tong, Y.; Tang, Q.; Liu, Y. Transport in organic single-crystal microbelt for conformal electronics. *Appl. Phys. Lett.* **2016**, *108*, 103502.
(62) James, D. T.; Kjellander, B. K. C.; Smaal, W. T. T.; Gelinck, G. H.; Combe, C.; McCulloch, I.; Wilson, R.; Burroughes, J. H.; Bradley, D. D. C.; Kim, J.-S. Thin-Film Morphology of Inkjet-Printed Single-Droplet Organic Transistors Using Polarized Raman Spectroscopy: Effect of Blending TIPS-Pentacene with Insulating Polymer. *ACS Nano* **2011**, *5*, 9824−9835.
(63) Huang, C.-W.; You, X.; Diemer, P. J.; Petty, A. J.; Anthony, J. E.; Jurchescu, O. D.; Atkin, J. M. Micro-Raman imaging of isomeric segregation in small-molecule organic semiconductors. *Commun. Chem.* **2019**, *2*, 22.
(64) Wood, S.; Hollis, J. R.; Kim, J.-S. Raman spectroscopy as an advanced structural nanoprobe for conjugated molecular semiconductors. *J. Phys. D: Appl. Phys.* **2017**, *50*, 073001.
(65) Desiraju, G. R.; Parthasarathy, R. The nature of halogen.-cntdot..cntdot..cntdot.halogen interactions: are short halogen contacts due to specific attractive forces or due to close packing of nonspherical atoms? *J. Am. Chem. Soc.* **1989**, *111*, 8725−8726.

(66) Thalladi, V. R.; Weiss, H.-C.; Bläser, D.; Boese, R.; Nangia, A.; Desiraju, G. R. C−H···F Interactions in the Crystal Structures of Some Fluorobenzenes. *J. Am. Chem. Soc.* **1998**, *120*, 8702−8710.
(67) Hunter, C. A.; Sanders, J. K. M. The nature of .pi.-.pi. interactions. *J. Am. Chem. Soc.* **1990**, *112*, 5525−5534.
(68) Hohenstein, E. G.; Duan, J.; Sherrill, C. D. Origin of the Surprising Enhancement of Electrostatic Energies by Electron-Donating Substituents in Substituted Sandwich Benzene Dimers. *J. Am. Chem. Soc.* **2011**, *133*, 13244−13247.
(69) Wheeler, S. E.; Houk, K. N. Substituent Effects in the Benzene Dimer are Due to Direct Interactions of the Substituents with the Unsubstituted Benzene. *J. Am. Chem. Soc.* **2008**, *130*, 10854−10855.
(70) Ostroverkhova, O.; Cooke, D.; Hegmann, F.; Anthony, J.; Podzorov, V.; Gershenson, M.; Jurchescu, O.; Palstra, T. Ultrafast carrier dynamics in pentacene, functionalized pentacene, tetracene, and rubrene single crystals. *Appl. Phys. Lett.* **2006**, *88*, 162101.

https://doi.org/10.1021/acs.chemmater.2c02534
Chem. Mater. 2023, 35, 81−93